Exosomes from human urine-derived stem cells ameliorate particulate polyethylene-induced osteolysis

Hui Li
Xiangya Hospital Central South University
Xiaolei Fan
Xiangya Hospital Central South University
Yinan Wang
Xiangya Hospital Central South University
Wei Lu
Xiangya Hospital Central South University
Haoyi Wang
Xiangya Hospital Central South University
Runzhi Liao
Xiangya Hospital Central South University
Min Zeng
Xiangya Hospital Central South University
Junxiao Yang
Xiangya Hospital Central South University
Jie Xie (dr_xiejie@163.com)
Xiangya Hospital Central South University https://orcid.org/0000-0001-8042-0600

Research Article

Keywords: exosomes, urine-derived stem cells, UHMWPE, Wear particle-induced osteolysis, anti-inflammation

Posted Date: February 23rd, 2021

DOI: https://doi.org/10.21203/rs.3.rs-238518/v1

Abstract

Background: Wear particle-induced periprosthetic osteolysis is a common long-term complication of total joint arthroplasty, and represents the major cause of aseptic loosening and subsequent implant failure. Currently, there are no effective therapeutic options to prevent osteolysis from occurring and often need revision surgery. Exosomes are important nano-sized paracrine mediators of intercellular communications and can be directly utilized as therapeutic agents for tissue repair and regeneration. Here, we explored the therapeutic potential of exosomes from human urine-derived stem cells (USC-Exos) in preventing wear particle-induced osteolysis.

Methods: USCs were characterized by flow cytometry and multiple differentiation potential. USC-Exos were identified by transmission electron microscopy (TEM), dynamic light scattering (DLS) and western blotting (WB). The impact of USC-Exos on osteoblastic differentiation of bone marrow mesenchymal stromal cells (BMSCs) and osteoclastogenesis of RAW264.7 cells were verified *in vitro*. The effects of USC-Exos on ultra high molecular weight PE (UHMWPE)-induced murine calvarial osteolysis model were tested to evaluate bone mass, inflammation, osteogenic and osteoclastic activities.

Results: USCs were positive for CD44, CD73, CD29 and CD90, but negative for CD34 and CD45. USCs were able to differentiate into osteogenic, chondrogenic, and adipogenic cells. USC-Exos exhibited a round-shaped morphology with a double-layered membrane structure and positive for CD63 and TSG101, negative for Calnexin. *In vitro*, USC-Exos could promote the osteogenic differentiation of BMSCs, reduces the production of proinflammatory factors in macrophages and suppresses their osteoclastic abilities. *In vivo*, injection of USC-Exos into the center of the calvariae caused less inflammatory cytokine generation and less osteolysis compared to control and significantly enhanced the bone formation.

Conclusions: Our findings demonstrate that USC-Exos can prevent UHMWPE-induced osteolysis by inciting less inflammatory, inhibiting bone resorption and stimulating bone formation. USC-Exos may represent a potential natural agent for the treatment of periprosthetic osteolysis and to obtain therapeutic exosomes for osteolytic treatment, aseptic loosening patients may just need to collect a certain volume of their own urine to harvest USCs and USC-Exos.

Introduction

Total joint arthroplasty (TJA) is a highly successful procedure in the case of severe joint diseases such as osteoarthritis, complex fractures, osteonecrosis and rheumatoid arthritis; TJA provides effect pain relief and improves the quality in patients' life with joint disease [1, 2]. Approximately 1.5 million joint arthroplasties are performed annually worldwide, and the demand for these surgeries is predicted to increase substantially [3]. Despite continuing technical innovation and a new understanding of biomechanics, a substantial decline in the revision rates has not occurred over the past decades [4]. Aseptic loosening, despite excellent outcomes of the joint arthroplasties, is the most common cause of arthroplasty component failure requiring revision arthroplasty, representing close to 75% of all cases, with

severe consequences for both the patient and the whole health-care system [5]. Although the pathophysiology of aseptic loosening is not completely explained, growing evidence suggests that periprosthetic osteolysis initiated by inflammatory responses to implant wear debris is responsible [6]. It is now well established that many particulates produced by prosthetic components, including PE, metal, alumina and polymethylmethacrylate (PMMA) are bioactive, and are therefore implicated in the initiation and or progression of osteolysis. However, periprosthetic osteolysis resulting from the generation of ultra high molecular weight polyethylene (UHMWPE) wear particles in artificial components is one of the major long-term complications following total joint arthroplasty [7]. The classic paradigm of periprosthetic osteolysis begins with the generation of wear particles that stimulate several different types of cells such as macrophages and T lymphocytes to secrete a variety of proinflammatory chemokines and cytokines, such as tumor necrosis factor-a (TNF-α), interleukin (IL)-1b, and IL-6 [8, 9]. These molecules in turn stimulate osteoclast precursors, and at the same time act on other target cells, mainly osteoblasts and bone marrow stromal cells, to promote their expression of receptor activator of nuclear factor-κB ligand (RANKL), a critical regulator of osteoclastogenesis. Upon binding to its receptor RANK on the surface of osteoclasts and their precursors, RANKL triggers activation of multiple intracellular signaling pathways to promote osteoclast differentiation and activity whereas suppressing its apoptosis. As a result, osteoclasts are excessively formed and activated at the bone-periprosthetic sites, eventually leading to extensive bone loss [8, 9]. The inflammatory reaction, bone resorption, and formation of foreign-body granulomas represent key processes leading to osteolysis [10]. Because osteoclasts are critical in the osteolytic process, compounds that specifically target functional osteoclasts are candidate agents for the prevention and treatment of wear particle-induced osteolysis and pathological bone loss. To date, no drug therapy to prevent or inhibit periprosthetic osteolysis has been approved, and aseptic loosening of prostheses can be overcome only by surgical revision.

Stem cell biology is a promising way that mains significant promise in the repair of injuries. Growing evidence indicates that most transplanted stem cells do not embed into the injured sites of recipient animal models, and a single injection of stem cells is sufficient to alleviate disease phenotypes and maintain therapeutic efficacy for a long time [11, 12], which suggests that paracrine action may be a key mechanism underlying the beneficial effects. Stem cells are capable of releasing different types of extracellular vesicles (EVs, 100–1,000 nm in diameter), such as exosomes, microvesicles, or microparticles [13]. Recently, exosomes, 30 - 150 nm in diameter, arising from the luminal membranes of multivesicular bodies (MVBs) and secreted into the extracellular milieu by most cell types through fusion with the cell membrane, have been of increased interest in the regenerative medicine field [13, 14]. Exosomes are composed of a lipid bilayer containing transmembrane proteins and enclosing cytosolic proteins and RNA. They can diffuse into the neighbouring cells or be carried via systemic transport to distant anatomic locations where they can induce signal transduction or mediate the horizontal transfer of information in specific recipient cells [13, 14]. Accumulating studies have revealed that direct treatment with these secreted vesicles can stimulate bone formation and avoid many risks associated with stem cell transplantation therapy [11, 15, 16]. However, the use of these stem cells is often limited by the source or genetic and epigenetic variations, and isolation of stem cells is also invasive and painful [17, 18, 19]. It

is imperative to look for a new stem cell source from which it is easy to obtain abundant exosomes for bone remodeling and regeneration.

It has been demonstrated that a subpopulation of stem cells can be easily isolated from human urine [17, 20, 21, 22, 23], i.e. urine derived stem cells (USCs). These cells possess biological characteristics with stem cell characteristics, such as cell surface marker expression profiles, clonogenicity, cell growth patterns, expansion capacity, multipotent differentiation, proangiogenic paracrine effects and easily-induced pluripotent stem cells [21]. A major advantage to using USCs is that these cells can be abundantly and noninvasively obtained. Chen et al used human urine-derived stem cells (USCs) to generate exosomes (USC-Exos) and found that USC-Exos could significantly promote osteogenesis and inhibiting osteoclastogenesis in osteoporotic mice [17]. Also USCs could serve as cell source for bone tissue regeneration. Guan et al. reported the ability of USCs seeded onto a β-tricalcium phosphate scaffold to induce bone healing in rats with femoral defects [24]. Considering that exosomes are important mediators of cell activity [13, 14], it would be interesting and meaningful to explore whether USC-Exos have the ability to prevent or inhibit osteolysis in the hope of identifying an innovative therapeutic strategy for attenuating UHMWPE-induced osteolysis to some extent.

In this study, we determined the effects of USC-Exos on osteogenic activity and osteoclast formation by coculturing exosomes with rat bone marrow mesenchymal stem cells (BMSCs) as well as mouse macrophages cell line RAW264.7. *In vivo*, we further verified the potential efficacy of USC-Exos to alleviate wear-debris-induced osteolysis in a murine osteolysis model. Our data indicated that the USC-Exos could prevent osteoclast differentiation and promote bone regeneration by inhibiting the inflammatory process and enhancing osteogenesis, potentially providing new ideas for treating periprosthetic osteolysis (Scheme 1).

Materials And Methods

Particle generation

UHMWPE particles (made available from Shamrock Tianjin TEDA, China) in the size range of 0.5 – 5 μm were used to model wear debris particles generated *in vivo* and *in vitro*. The particles had a mean diameter of 3.8 μm. Macrophage inflammatory response to wear particles has been shown to depend on the size and shape of the wear particles with particles in the size range of 0.5 – 5 μm eliciting a strong inflammatory response [25].

The particles were rinsed in 70% ethanol and 100% ethanol respectively, and were sterilized with cobalt 60γ - radiation in a vacuum. PE are white micronized powder and have a density of 0.97 g/cm^3, thus the particles were suspended in absolute ethanol firstly. The particle suspension was determined to be endotoxin free using a BIOENDO Endotoxin Quantitation Kit (Xiamen Bioendo Technology Co., Ltd., Xiamen, China). The size distribution and Zeta potential of UHMWPE was measured by dynamic light scattering (DLS) with a Nanosizer™ instrument (Malvern Instruments, Malvern, UK).

Mouse macrophage culture and co-culture of macrophages and PE particles

RAW 264.7 mouse macrophage cells were cultured in high glucose DMEM (Shanghai BasalMedia Technologies Co., Shanghai, China) supplemented with 10% FBS (Gibco) and 1% penicillin-streptomycin (Gibco) at 37℃ in a humidified 95% air/5% CO_2 atmosphere. Because UHMWPE density is less than water, PEs float on the surface of the cell culture media, presenting a challenge to a conventional experimental set-up. A number of studies have used various techniques to confine UHMWPE to the bottom of well plates such as inverted cell culture, but the system have several disadvantages: 1) it increases the probability of cell contamination when changing the cell culture media; 2) most importantly the experimental methods is not simple [26, 27]. We have therefore suspended sterilized UHMWPE in culture medium, then boasted and aspirated repeatedly the medium with a pipette for 30 minnutes until the color of the medium became pink.

Isolation, culture and identification of human USCs

The isolation and characterization of USCs were performed as described previously [17, 23]. The process of collection and isolation of urinary cells was showed in Fig. S1. Briefly, the mid-stream of human urine samples (50 mL) were collected into a sterile 50 mL tube containing 500 µL Antibiotic-Antimycotic (100 x stock; Gibco, Grand Island, USA) from a healthy male donor with age of 30 years. Then transferred the 50ml urine into four 15ml tube, after centrifugation at 400 x g for 10 min, the supernatant was aspirated and only 1 mL was left in the bottom of tube. 10 mL sterile PBS was added to the tube, after centrifugation at 200 x g for another 10 min, the supernatant was carefully discarded, leaving only 0.2 mL plus the pellet. All procedures were performed at room temperature. The cell pellet was resuspended in 1 mL primary medium (Lonza, USA) and transferred into one wells of a 12-well plate. Cells were maintained at 37 °C in a humidified atmosphere containing 5% CO_2. Check the plates under the microscope (Leica DMI6000B, Solms, Germany) daily and continue to incubate until cells reach 80–90% density. Early-passage USCs (p2-6) were used for the downstream experiments.

Multipotent differentiation potentials (including osteogenesis, adipogenesis and chondrogenesis) of USCs were evaluated by using the osteogenic, adipogenic and chondrogenic differentiation media (Cyagen Biosciences, Guangzhou, China) as described previously [17, 28]. The expression of surface marker proteins (including CD29-PE, CD44-FITC, CD73-PE, CD90-APC, CD34-FITC and CD45-FITC) on Passage 4 USCs was detected by flow cytometry as described previously. [17] Results were analyzed with Flowjo software (Tree Star Inc, Ash-land, USA). All antibodies were obtained from BD Biosciences (San Jose, CA, USA).

Isolation and identification of USC-Exos

USCs-Exos were isolated from culture medium using a protocol modified from a previous study [17, 29]. The process of isolation and characterization of USCs-Exos was showed in Fig. S2. After reaching 70-80% confluence, USCs were washed with PBS and incubated with freshly prepared complete medium (Lonza, USA) containing exosome depleted fetal bovine serum (Shanghai VivaCell Biosciences Ltd,

Shanghai, China) for 48 h. The conditioned medium of USCs was collected and centrifuged at 300 ×g for 10 min, 2000 ×g for 30 min, and 4000 ×g for 30 min. Then the supernatant was filtered using a 0.22 μm filter (Millipore, Billerica, USA). 15 mL supernatant was added to an Amicon Ultra-15 Centrifugal Filter Unit (10 kDa; Millipore) and centrifuged at 4000 ×g to about 1 mL. One-fifth volume of Exoquick Exosome Precipitation Solution (System Biosciences, USA) was added to the ultrafiltration liquid and mixed well by inverting. After incubation for 12 h, the mixture was centrifuged at 1500 ×g for 30 min and the supernatant was removed by aspiration. The exosome pellets were resuspended in 100-200 μL PBS according to the volume of exosome pellets. All procedures were performed at 4 ºC. The protein content of exosomes was determined by the BCA Protein Assay Kit (Multi Sciences LTD., Hangzhou,China). Exosomes were stored at -80 °C or used for the downstream experiments.

To identify the isolated exosomes, western blotting analysis was conducted to detect the expression of rabbit anti-TSG101 (ab125011, 1:1000, Abcam), mouse anti-CD63 (sc-5275, 1:500, Santa) and rabbit anti-calnexin (ab22595, 1:1000, Abcam) as described previously in detail [17, 30]. Cell extract was used as control. Dynamic light scattering (DLS) with a Nanosizer™ instrument (Malvern Instruments, Malvern, UK) was used to identify the size distribution of USC-Exos. Exosomes morphologies were observed by TEM (Hitachi H7500 TEM, Tokyo,Japan) as described previously in detail [17, 31]. Briefly, exosomes were loaded onto a copper grid. After staining with 2% (w/v) phosphotungstic acid for 5 min, the sample was examined by TEM.

Exosomes uptake assay

To determine whether RAW264.7 can uptake USC-Exos, we stained exosomes with PKH26 fluorescent dye (Sigma) according to the manufacturer's instruction. Exosomes (800 μg) diluted in PBS were added to 1.0 ml Diluent C. In parallel, 4μl PKH26 dye was added to the exosome solution for 5 minutes at room temperature while avoiding light. Cells were seeded on glass coverslips pretreated with TC (Solarbio) and cultured for 24 h to reach 80 – 90% confluency. We then co-culture a total of 25μL (100 ug) USC-Exos with RAW264.7 in serum-free media. Images were captured with fluorescence microscope (Leica, Germany).

Osteoclastic differentiation assay

The osteoclast progenitor RAW264.7 cells were plated in 48-well culture plates at 1.0×10^4 cells per well and incubated overnight. After that, the medium were randomized into the following treatment conditions：1) Vehicle group (DMEM + PBS); 2) UHMWPE + RANKL + vehicle group (DMEM + UHMWPE + RANKL + PBS); 3) UHMWPE + RANKL + USC-Exos group (DMEM + RANKL + PBS). The medium was changed to fresh complete DMEM or DMEM + UHMWPE containing 100 ng·mL-1 RANKL (ProteinTech, Chicago, USA) and 300 μg·mL-1 USC-Exos or vehicle (PBS). The culture medium was changed every 2 days. After 7 days of induction, the cells were washed with PBS and fixed in 4% PFA for 10 min. Osteoclasts were stained using a commercially TRAP Kit (Sigma) and then quantified using an inverted microscopy (Leica). The numbers of $TRAP^+$ osteoclasts (> 3 nuclei) in each well were counted under a

microscope (Leica). After 4 days of induction, the CM were harvested and centrifuged at 2000 ×g for 10 min to collect the supernatant, which was stored at –80 °C or used for ELISA.

Osteogenic differentiation assay

BMSCs were isolated from 4-week-old male C57BL/6 mice. Briefly, bone marrow cells were obtained from the femurs and tibia of mice. After rinsing by centrifugation, cells were resuspended in α-MEM (Gibco, Grand Island, USA) containing 10% FBS (Gibco), 1% penicillin (100 U/mL, Gibco) and streptomycin (100 μg/mL, Gibco). BMSCs were plated in 48-well plates at 1.0×10^5 cells per well. After 24 h, the cells were cultured in osteogenesis induction medium (Cyagen Biosciences Inc, Santa Clara, USA) + UHMWPE (1.0 mg/ml) treated with or without USC-Exos (100 μg/ml). The medium was changed every two days. 4 days later, the conditioned media were obtained and centrifuged at 2000 × g for 10 min to remove cellular debris. Then the supernatant was assayed with an Alkaline phosphatase assay kit and Calcium assay kit according to the manufacturer's protocol (Nanjing Jiancheng Bioengineering Institute, Nanjing, China). After 12 days of induction, the cells were washed with PBS, fixed in 4% PFA for 10 min, and then stained with Alizarin Red S (ARS) solution (Cyagen Biosciences Inc, Santa Clara, USA). An inverted microscope (Leica DMI6000B, Solms, Germany) was used for imaging.

Western blotting

5× protein-loading buffer (5×; Beyotime Biotechnology, Jiangsu, China) was added directly to the lysates of USCs or exosomes and heated at 95 ºC for 5 min. Next protein extracts were loaded and resolved in 12% SDS-PAGE. The protein sample was run at 120 V for 45 minutes and transferred onto polyvinylidene difluoride membranes (Immobilon P, Millipore, USA) for 1.5 hours at 100 mA. The membranes were incubated with primary antibodies at 4 ºC overnight and then incubated with the secondary antibodies at room temperature for 1 h. Primary antibodies and dilutions were used as follows: anti-CD63 (sc-5275, 1:500, Santa), TSG101 (ab125011, 1:1000, Abcam) and Calnexin (ab22595, 1:1000, Abcam). All the secondary antibodies (1:5000) were obtained from Cell Signaling Technology. The immunoreactive bands were visualized using enhanced chemiluminescence reagent (Thermo Fisher Scientific, Waltham, USA) and imaged by the ChemiDoc XRS Plus luminescent image analyser (Bio-Rad).

UHMWPE-induced calvarial osteolysis model and surgical treatment

Animal care and experimental procedures were approved by the Department of laboratory Animal Management Committee of Central South University (No. 2020sydw0972). Thirty female BALB/c mice (8 - 10 weeks old) were purchased from Hunan SJA Laboratory Animal Company (Changsha, China). Each mouse weighed 20-24 g at the beginning of the experiment. The *in vivo* calvaria experiments were performed with reference to similar previous experiments [32] with a little modification. Briefly, mice were anesthetized by intraperitoneal injection of ketamine and xylazine following the standard protocol. Following anesthesia, skin on the calvariae was shaved, disinfected and then incised with a sharp scalpel along the middle line. Subsequently, 30 mg of UHMWPE particles were evenly spread on the surfaces of the bilateral parietal bones, followed by closure of the surgical skin incision using 4-0 Prolene sutures. A

total of 30 mice were randomly assigned to three experimental groups of 10 each: Vehicle control (sterile PBS), UHMWPE group, UHMWPE + USC-Exos group. After subcutaneously injected to the center of the calvariae once postoperation, USC-Exos injections continued to be given once a week for another three times, and the control mice were local injected with PBS (the vehicle of USC-Exos). The mice were sacrificed in a carbon dioxide chamber at day 28 and their calvariae were isolated and fixed with 4% PFA for 2 days. After fixation, calvarial samples were washed three times with PBS and then stored in PBS at 4 °C until further analysis.

In Vivo Fluorescent Imaging for Biodistribution of USC-Exos

USC-Exos (800 μg) were incubated with DiR (D12731 ,Thermo Fisher Scientific) for 20 min in a final volume of 500 μl at 37℃ while avoiding light, then washed with PBS, and the samples were then processed as with the PKH26 dye in front. The BALB/c mice were anaesthetized by intraperitoneal injection of pentobarbital (50 mg/kg) and USC-Exos -DiR (n = 3) or PBS (n = 3) was subcutaneously injected to the center of the calvariae. Fluorescence images were obtained after day 1, day 3, day 6, day 8, day 10, day 13 and day 15 by a fluorescence tomography imaging system (FMT-4000; PerkinElmer, USA). 15 days after the injection, the mice were sacrificed for *ex vivo* tissue distribution analysis.

Micro-CT analysis

μCT was used to quantitatively evaluate the bone mass. The cranium were dissected from mice, fixed for 48 hours in 4% paraformaldehyde (PFA) and analyzed by high-resolution μCT (Skyscan 1176; Skycan, Aartselaar, Belgium). The voltage, current, and resolution were set to 50 kV, 400 μA, and 8.88 μm per pixel, respectively. For quantitative analysis, 100 μCT slices in the center of each calvaria were used, and region of interest (ROI) was selected as previously described. [32] CTAn software (SkyScan, Aartselaar, Belgium) was utilized to generate three-dimensional (3D) images and calculate the percentage of bone volume out of total tissue volume (BV/TV). 3D μCT images were visualized using Mimics v10.01 software (Materialise, Leuven, Belgium). The number of pores and percentage of porosity were counted by ImagePro plus 6.0 software.

Histological and immunohistochemical analysis

After micro-CT scanning, the calvaria samples were decalcified in 10% EDTA (pH 7.4) (Amresco, Solon, OH, USA) for 5 days and embedded in paraffin. Tissue coronal sections at the middle level (5 μm) were stained with hematoxylin & eosin (H&E) to evaluate the degree of bone erosion. Three separate sections per specimen were evaluated in a blinded fashion. The regions containing the discontinuous and non-osseous tissues were considered as the osteolytic areas, and selected for histomorphometric analyses. The periosteum thickness (mm) were measured and quantified. Osteoclast-like cells were identified by histochemical tartrate-resistant acid phosphatase (TRAP) staining using a commercial kit (Sigma-Aldrich, St. Louis, MO) to identify the the number of osteoclasts. The percentage of osteoclast surface per bone surface (OCs/BS, %) were determined for each sample. The stained sections were examined under a light microscope (Olympus CX31; Olympus Optical Co., Tokyo, Japan) and digital photomicrographs were

captured and analyzed using a computerized image analysis system with Image-Pro Plus software, version 6.0 (Media Cybernetics, Silver Spring, MD, USA).

For immunofluorescence staining for OCN and TNF-α, the sections were rehydrated and heated in a microwave in citrate buffer (0.01 M; pH 6.0) for 15 min to retrieve the antigen. The sections were then blocked in 1.5% normal goat serum for 30 min at room temperature, incubated with the primary antibodies anti-OCN (1:100; Abcam) or anti-TNF-α (1:500; Abcam)overnight at 4°C, and then incubated with the respective secondary antibodies (1:250; Abcam) at room temperature for 1 h while avoiding light. The color was developed by adding 3,30-diaminobenzidine tetrahydrochloride (DAB). In negative control sections, the primary antibody was replaced with 1.5% normal goat serum. Images were acquired with a fluorescence microscope (Leica). Relative staining intensity or positively stained cell number were measured in three random visual fields per section, three sequential sections per mouse and three mice in each group.

Safety examination

To determine the immunogenicity of the USC-Exos, the blood was collected after anesthesia and subsequently analyzed by hematology and blood chemistry tests. The safety of the USC-Exos was further evaluated by examining the main organs via histological sectioning and H&E staining. Samples from untreated mice were used as controls.

Enzyme-linked immunosorbent assay (ELISA)

The concentrations of TNF-α and IL-6 in the CM were measured using a commercial Mouse TNF-α ELISA Kit (ab208348, Abacam) and a Mouse IL-6 ELISA Kit (ab222503, Abacam) according to the protocol provided by the manufacturer. The optical density of each well was determined using a microplate reader (Bio-Rad 680, Hercules, USA) set to 450 nm. Wavelength correction was set to 570 nm. The protein concentration for each sample was calculated according to the standard curve.

Statistical analysis

Data are presented as mean ± standard deviation (SD). Statistical analysis of multiple-group comparisons was analyzed by one-way analysis of variance (ANOVA), followed by the Bonferroni *post hoc* test to assess the significance of differences between two groups. Analyses were performed using Prism 8.0 software. Differences were judged to be statistically significant when $P \leq 0.05$.

Results

UHMWPE microparticle characterization

Morphology, size distribution and Zeta potential of UHMWPE was determined by scanning electron microscopy (SEM) and DLS (Fig. 1A, 1B, 1C). A representative SEM image of the UHMWPE depicts the characteristic irregular shape and rough surface of these particles (Fig. 1A). On the basis of size

distributions, over 90% of the particles were in the size range of 0.5 - 5 μm (Fig. 1B). The Zeta potential is “slightly negative” (Fig. 1C), this “slightly negative” Zeta potential is ideal for cytophagy. The curve of endotoxin were as presented in Fig. 1D, and the detection of the UHMWPE endotoxin concentration at 2 h is 0.052 EU/mL.

Identification of USCs and USC-Exos

Single, small, compact“rice-grain” like cells was observed 2-3 days after initial seeding (Fig. S3). A few days after being placed in a well a single cell formed a cluster of cells that appeared small, compact and uniform (Fig. S3). Cell colonies were observed in the USCs cultured plates approximately 3 to 10 days after initial plating (Fig. S3). After 12 days, the fibroblast-like cells retained a robust proliferation capability and reached 80%-90% confluence (Fig. S3). Most of the adherent cells exhibited a fibroblast-like morphology (Fig. 2A). Fig. 2B reveal that after culturing in specific induction medium, USCs demonstrated to differentiate into an osteogenic, chondrogenic or adipogenic lineage as indicated by the positive staining for Alizarin Red, toluidine blue and Oil Red O, respectively. Moreover, the CCK-8 assay showed that the cells underwent a rapid growth phase from day 3 to day 7 and the growth slowed down after day 7 (Fig. 2C). In addition, flow cytometry results showed that USCs were highly positive for MSC surface markers including CD29, CD44, CD73 and CD90, but negative for CD34 and CD45 (Fig. 2D). The data indicated that cells isolated from human urine and maintained under specific culture conditions were classified as MSC [17, 20, 33, 34]. The morphology of exosomes was observed using TEM (Fig. 2E), which revealed that the particles were a sphere-shaped morphology with a double-layered membrane structure, similar to previously described [13, 17, 35]. Second, the size distribution of the extracellular particles measured by DLS demonstrated that these particles predominantly ranged from 30 nm to 100 nm (Fig. 2G), which was corresponding with the previously reported exosomes size distributions [13, 17, 35]. Finally, western blotting results showed that USCs-Exos were positive for exosomal specific markers CD63 and TSG101, and were negative for Calnexin (Fig. 2F).

Internalization of exosomes by RAW 264.7

To investigate whether exosomes could enter into the cytoplasm of RAW 264.7, we incubated the labeled exosomes with RAW 264.7. Fluorescence microscopy analysis (Fig. 3B) showed that the USC-Exos labelled with PKH-26 (the red dots) was internalized by the RAW 264.7. At 24h post incubation, a large number of exosomes have been internalized and distributed in the perinuclear region.

USC-Exos inhibit osteoclast formation and downregulate inflammatory cytokines

1 mg/ml UHMWPE were cultured with RAW 264.7, and results showed that: (1) RAW 264.7 cells are capable to phagocyte particle (dark dots), as shown in Fig. 3A; (2) the concentration of particles did not seriously affect the cell viability (Fig. 3C).

To examine the effects of USC-Exos on osteoclastogenesis and the production of inflammatory cytokines, osteoclast precursor cell line RAW264.7 cells were induced by the osteoclastogenic factor

RANKL and treated with USC-Exos or vehicle (PBS) for 7 days. TRAP staining revealed that RAW264.7 cells cultured with RANKL and UHMWPE exhibited a large amount of $TRAP^+$ mononuclear preosteoclasts and multinucleated osteoclasts, whereas USC-Exos treatment inhibited osteoclast formation and caused the accumulation of preosteoclasts (Fig. 3D, 3E). As evidenced by ELISA, the concentration of TNF-α and IL-6 in CM from RNAKL + UHMWPE induced cells was much higher than that in the un-induced group, and USC-Exos treatment resulted in a further decrease of TNF-α and IL-6 production (Fig. 3F). Our results suggest that USC-Exos inhibit osteoclast formation by decreasing the concentrations of inflammatory cytokines.

USC-Exos enhance osteogenic activities

To evaluate the effects of USC-Exos on osteoblasts *in vitro*, BMSCs were cultured in osteogenesis induction medium supplemented with USC-Exos or PBS. The concentration of ALP and Ca^{2+} were analysed to determine the osteoblastic differentiation of BMSCs after 3 days of induction (Fig. 3G). As illustrated in Fig. 3H, the USC-Exos enhanced matrix mineralization and the concentration of ALP, Ca^{2+} were significantly higher than the vehicle group. Alizarin Red S (ARS) staining revealed that USC-Exos markedly enhanced the calcium nodule formation of MSCs (Fig. 3H). The results of the concentration ALP, Ca^{2+} and ARS staining showed that USC-Exos promoted osteoblastic differentiation of BMSCs.

Biodistribution of USC-Exos in murine calvarial osteolysis model

To investigate the local biodistribution of USC-Exos, we first employed the mouse model of calvarial bone resorption, and then stained exosomes with DiR and injected them into the center of calvariae. The mice were imaged using the IVIS at indicated time and we observed that the fluorescence intensity of DiR-labled USC-Exos gradually decrease within 2 weeks, but the fluorescence could still be detected locally in the calvariae at the end point (Fig. 4A, 4B). Then the major organs including the calvariae were taken out and observed. We found that DiR-labled USC-Exos cannot be detected in the lungs, hearts,livers, spleens, and kidneys of the treated animals, but can be detected in the calvariae (Fig. 4C). These data indicate that the local injection of USC-Exos could sustain about 2 weeks.

USC-Exos prevents UHMWPE-induced osteoclastic bone resorption

As seen in Fig. 5A, the gross pathology verified that UHMWPE particle developed a pronounced inflammatory response in the calvariae. To explore the biological effect of USC-Exos on pathological osteolysis, we examined how USC-Exos affected UHMWPE-induced osteolysis in a murine calvarial model. By performing micro-CT scans and 3D reconstruction, we determined that extensive bone resorption occurred in the UHMWPE group, which was observed as extensive surface erosions on the calvaria, when compared with the negative control (Sham; PBS injection) (Figure. 5B). However, treatment with USC-Exos suppressed UHMWPE induced osteolysis (Fig. 5B). Quantifification of bone parameters confirmed that USC-Exos signifificantly increased the BV/TV (Fig. 5C) and decreased the number of pores and percentage of porosity (%) (Fig. 5D, 5E).

Histological assessment and histomorphometric analysis further confirmed that USC-Exos treatment protected against UHMWPE-induced bone loss. The H&E staining showed that sections in the sham-group exhibited few osteolytic changes. In the vehicle group, osteolysis had clearly occurred, whereas the USC-Exos-treated groups exhibited reduced osteolysis (Fig. 6A), and the area of eroded surface and thickness of periosteum were lower than in the UHMWPE-induced group, respectively (Fig. 6B, 6C). Furthermore, in accord with the micro-CT quantitation, histomorphometric analysis demonstrated that USC-Exos reduced the erosion surface. TRAP staining revealed that the number of multinucleated osteoclasts in the injection site was increased in response to the presence of UHMWPE particles, which was indicated by the presence of osteoclasts that lined the eroded bone surface. However, in USC-Exos-treatment groups, the number of osteoclasts and the percentage of osteoclast surface relative to bone surface decreased (Fig. 6D, 6E, 6F), which indicates that USC-Exos treatment inhibited osteoclast formation during UHMWPE induced osteolysis *in vivo*. The results of immunohistochemical staining are shown in Fig. 6D. We found that the osteogenic markers OCN were highly expressed in the USC-Exos treatment group (Fig. 6G). In addition, decreased amounts of TNF-α expression were quantifified in the USC-Exos group (Fig. 6H).

Safety of USC-Exos

Major concerns about the application of exosomes from human urine sample are immunogenicity. The safety of the USC-Exos was evaluated by testing the function of red blood cells and performing a histological examination of the major organs (Fig. 7A). The proportions of white blood cells and platelets showed no significant differences after USC-Exos treatment (Fig. 7B). Moreover, the proportions of differential white blood cells (including neutrophils, lymphocytes, monocytes, eosinophils, basophils) were calculated and showed no significant differences. As shown in Fig. 7C, the concentration of hemoglobin in the blood (HGB), the mean corpuscular hemoglobin (MCHC) level and the hemoglobin distribution width (HDW) were quite similar among the groups, indicating that the USC-Exos did not influence the function of red blood cells. H&E staining of the brain, heart, lung, liver, spleen and kidneys further revealed no obvious pathological changes among the groups. (Fig. 7D).

Discussion

Total joint arthroplasty (TJA) is commonly used to treat the most severe joint diseases. However, periprosthetic osteolysis and aseptic loosening following TJA is a complex problem that requires meticulous evaluation and preoperative planning. Wear particles and the biological effects of wear debris have a major effect on biological parameters in the periprosthetic environment, which are currently among the most serious problems in patients undergoing arthroplasty surgery. PE particles produced by an artificial joint have been increasingly recognized as having the potential to induce inflammation and osteolysis [36, 37, 38], which would directly result in failure of artificial joint replacement. Revision TJA is related to surgical and implant demands as bone defects need to be repaired and joint stability has to be restored. In addition, revision surgery is associated with increased patient morbidity, and great economic burden for the health care system [39, 40]. In this study, we found that USC-Exos could effectively

promoted osteoblast formation and inhibit osteoclast formation *in vitro*. We also noted that USC-Exos induced lower inflammatory cytokines compared to the control. *In vivo*, we demonstrated that local injection of USC-Exos could effectively alleviate bone loss in mice, as defined by increased trabecular and cortical bone mass, enhanced osteogenic activities and reduced osteoclast formation. Our findings suggest a promising future prospect for autologous USC-Exos to be used as a new treatment for periprosthetic osteolysis patients. That is, to obtain therapeutic exosomes for osteolytic treatment, aseptic loosening patients may just need to collect a certain volume of their own urine to harvest USCs.

Over the past years, the application of pluripotent stem cells for bone tissue engineering has received much attention among researchers and clinicians [41, 42, 43]. USCs is one of the most promising stem cell resource and have therapeutic potential for many bone diseases [24, 42]. Recent studies have demonstrated that transplantation of stem cells contributes to tissue repair and regeneration not by the direct differentiation into the parenchymal cells, but rather by the paracrine effects to stimulate endogenous cells participating in tissue regeneration [11, 12, 44, 45]. Exosomes are crucial paracrine mediators obtained from most cell types in culture and biological fluids including plasma, milk, amniotic fluid, pleural effusions. All extracellular vesicles bear surface molecules that allow them to be targeted to the recipient cells. Once attached to target cell, extracellular vesicles can induce intracellular signaling via receptor-ligand interaction or can be internalized by endocytosis and/or phagocytosis or even fuse with the target cell's membrane to deliver their contents into its cytoplasm, thereby modifying the physiological state of the recipient cell [13]. Stem cells-derived exosomes possess therapeutic effects in various disease models similar to their original cells [46], suggesting that exosomes are critical effectors of stem cells. Qi et al. indicated that exosomes released by human-induced pluripotent stem Cell-derived MSCs promoted bone regeneration of critical-sized calvarial defects in osteoporosis rat [16]. Zhang et al. demonstrated that mesenchymal stromal cells-generated exosomes effectively ameliorate functional recovery by promoting endogenous angiogenesis and neurogenesis, reducing inflammation in rats after TBI [47]. Hu et al. indicated that extracellular vesicles released by human umbilical cord blood could ameliorate bone loss in senile osteoporosis mice [41]. Chen et al. reported that extracellular vesicles from human urine-derived stem cells effectively alleviates bone loss and maintains bone strength in osteoporotic mice [42]. These results provided evidences that exosomes could be used to stimulate bone repair in bone diseases. A large number of studies have reported the function of urine-derived stem cells on tissue regeneration [17], whereas few studies have directly utilized USCs to isolate extracellular vesicles for therapeutic uses. Herein, we harvested exosomes from human USCs and verified that USC-Exos could ameliorate bone loss of mouse osteolysis model, indicating that USC-Exos might be utilized as a new non-operative therapeutic interventions for the treatment of aseptic loosening.
The inflammatory reaction, bone resorption, and formation of foreign-matter granulomas around the bone-prosthesis site is the principal pathophysiological mechanism of aseptic loosening [10], while monocytes/macrophages represent the critical cell type closely coupled with this pathophysiological process. RAW 264.7 cell is also frequently employed in *in vitro* models for evaluating cellular phenomena related to exposure to wear debris [9]. RAW 264.7 is a mouse monocyte/macrophages cell line that represents an ideal osteoclasts precursor, as its expression profile is very close to the osteoclasts, and

also because these cells are able, once properly stimulated by RANKL cytokines only, to resorb bone [48]. BMSCs are the major source of osteoblasts that contribute to bone formation [49]. In this study, we demonstrated that USC-Exos could be internalized by RAW264.7 and remarkably inhibited the osteoclast differentiation of RAW264.7 as evidenced by decreased number of osteoclasts, while accelerated osteoblastic differentiation of BMSCs as defined by ARS staining and increased ALP activity and matrix mineralization. In addition, an adequate blood supply is important for bone formation and maintenance [50] and Chen at al. previously confirmed that USC-Exos are able to transfer proangiogenic proteins to endothelial cells and thereby promote angiogenesis [17]. Therefore, USC-Exos may be a feasible and effective therapeutic candidate to treat or prevent wear debris–associated osteolysis and aseptic loosening.

At present, major concerns regarding the application of USC-Exos are immunogenicity and safety. Nevertheless, if we can test the immunogenicity of USC-Exos, then it will be useful to evaluate their safety when the use of allogeneic or heterogeneic USC-Exos is required. The safety of the USC-Exos was evaluated by testing the function of red blood cells and performing a histological examination of the major organs. In our study, we found that human USC-Exos did not evoke obvious immune responses in recipient mice between USC-Exos-treated mice and vehicle-treated control mice. However, we did not test the levels of antibodies against USC-Exos in these mice after the long-term use of these heterogeneic USC-Exos. Future studies are required to comprehensively and systematically assess the immunogenicity of USC-Exos.

Conclusions

In conclusion, our results demonstrate that USC-Exos are able to ameliorate bone loss in osteolysis mice. The potential mechanism is the inhibition of inflammatory cytokines and the regulation of function properties of osteoblasts and osteoclasts, as USC-Exos can promote osteogenic differentiation of BMSCs and inhibit osteoclastic differentiation of osteoclast precursor cells *in vitro*. Our data suggest that USC-Exos may represent a novel therapeutic tool for orthopaedic wear-debris associated osteolysis.

Abbreviations

USCs: urine-derived stem cells; Exos: exosomes ; USC-Exos: exosomes from urine-derived stem cells; MVBs: multivesicular bodies; MSCs: mesenchymal stem cells; PBS: phosphate-buffered saline; FBS: fetal bovine serum; ARS: alizarin red S; CCK-8: cell counting kit-8; H&E: hematoxylin and eosin; WB: Western blotting.

Declarations

Author Contributions

Jie Xie designed experiments. Hui Li, Xiaolei Fan, Yinan Wang, Wei Lu, Haoyi Wang and Runzhi Liao conducted experiments, animal modeling assistance. Hui Li provided the urine samples, collection and/or assembly of data, data analysis and interpretation, manuscript writing. Min Zeng, Junxiao Yang provided technical support. All authors reviewed and agreed the manuscript.

Funding

This work was supported by the National Natural Science Foundation of China (Grant No. 81974339), the Science and Technology Plan Project of Hunan Province (Grant Nos. 2019JJ40499).

Availability of data and materials

The data generated or analyzed during this study are included in this article, or if absent are available from the corresponding author upon reasonable request.

Ethics approval and consent to participate

This study was approved by the Department of laboratory Animal Management Committee of Central South University (No. 2020sydw0972) and was conducted according to all current ethics guidelines.

Consent for publication

Not applicable.

Competing interests

The authors declare no conflict of interests.

References

1. Tian B, Jiang T, Shao ZY, Zhai ZJ, Li HW, Fan QM, Liu XQ, Ouyang ZX, Tang TT, Jiang Q, Zheng MH, Dai KR, Qin A, Yu YP, Zhu ZN. The prevention of titanium-particle-induced osteolysis by OA-14 through the suppression of the p38 signaling pathway and inhibition of osteoclastogenesis. Biomaterials, 2014, 35(32):8937-50.
2. Zhang LW, Yang YJ, Liao ZR, Liu QB, Lei XH, Li M, Saijilafu, Zhang ZY, Hong D, Zhu M, Li B, Yang HL, Chen JQ. Genetic and pharmacological activation of Hedgehog signaling inhibits osteoclastogenesis and attenuates titanium particle-induced osteolysis partly through suppressing the JNK/c-Fos-NFATc1 cascade. Theranostics, 2020, 10(15):6638-6660.
3. Gallo J, Goodman SB, Lostak J, Janout M. Advantages and disadvantages of ceramic on ceramic total hip arthroplasty: a review. Biomed Pap Med Fac Univ Palacky Olomouc Czech Repub. 2012; 156: 204-12.
4. Thiele K, Perka C, Matziolis G, Mayr HO, Sostheim M, Hube R. Current failure mechanisms after knee arthroplasty have changed: polyethylene wear is less common in revision surgery. J Bone Joint Surg

Am. 2015; 97: 715-20.

5. Malchau H, Herberts P, Eisler T, Garellick G, S¨oderman P. The Swedish Total Hip Replacement Register. J Bone Joint Surg Am. 2002;84(S2)(Suppl 2):2-20.
6. Camuzard O, Breuil V, Carle GF, Pierrefite-Carle V. Autophagy Involvement in Aseptic Loosening of Arthroplasty Components. J Bone Joint Surg Am. 2019; 101: 466-472.
7. Ingham E, Fisher J. The role of macrophages in osteolysis of total joint replacement. Biomaterials 2005;26:1271-86.
8. Wu C, Wang W, Tian B, Liu X, Qu X, Zhai ZJ, Li HW, Liu FX, Fan QM, Tang TT, Qin A, Zhu ZA. Myricetin prevents titanium particle-induced osteolysis in vivo and inhibits rankl-induced osteoclastogenesis in vitro. Biochem Pharmacol. 2015; 93: 59-71.
9. Nich C, Takakubo Y, Pajarinen J, Ainola M, Salem A, Sillat T, Rao AJ, Raska M, Tamaki Y, Takagi M, Konttinen YT, Goodman SB, Gallo J. Macrophages-key cells in the response to wear debris from joint replacements. J Biomed Mater Res A. 2013; 101: 3033-45.
10. Drees P, Eckardt A, Gay RE, Gay S, Huber LC. Mechanisms of disease: molecular insights into aseptic loosening of orthopedic implants. Nat Clin Pract Rheumatol. 2007; 3: 165-71.
11. Liu S, Liu D, Chen C, Hamamura K, Moshaverinia A, Yang R, Liu Y, Jin Y, Shi S. MSC transplantation improves osteopenia via epigenetic regulation of Notch signaling in lupus. Cell Metab. 2015; 22: 606–618.
12. Lavasani M, Robinson AR, Lu A, Song M, Feduska JM, Ahani B, Tilstra JS, Feldman CH, Robbins PD, Niedernhofer LJ, Huard J. Muscle-derived stem/progenitor cell dysfunction limits healthspan and lifespan in a murine progeria model. Nat. Commun. 2012; 3: 608.
13. Tkach M, Thery C. Communication by Extracellular Vesicles: Where We Are and Where We Need to Go. Cell. 2016; 164: 1226-32.
14. Syn N, Wang L, Sethi G, Thiery JP, Goh BC. Exosome-Mediated Metastasis: From Epithelial-Mesenchymal Transition to Escape from Immunosurveillance. Trends Pharmacol Sci. 2016 ;37: 606-617.
15. Hu Y, Xu R, Chen CY, Rao SS, Xia K, Huang J, Yin H, Wang ZX, Cao J, Liu ZZ, Tan YJ, Luo J, Xie H. Extracellular vesicles from human umbilical cord blood ameliorate bone loss in senile osteoporotic mice. Metabolism. 2019; 95: 93-101.
16. Qi X, Zhang J, Yuan H, Xu Z, Li Q, Niu X, Hu B, Wang Y, Li X. Exosomes secreted by human-induced pluripotent stem cell-derived mesenchymal stem cells repair critical-sized bone defects through enhanced angiogenesis and osteogenesis in osteoporotic rats. Int. J. Mol. Sci. 2016; 12: 836–849.
17. Chen CY, Rao SS, Tan YJ, Luo MJ, Hu XK, Yin H, Huang J, Hu, Y, Luo ZW, Liu ZZ, Wang ZX, Cao J, Liu YW, Li HM, Chen Y, Du W, Liu JH, Zhang Y, Chen TH, Liu HM, Wu B, Yue T, Wang YY, Xia K, Lei PF, Tang SY, Xie H.Extracellular vesicles from human urine-derived
stem cells prevent osteoporosis by transferring CTHRC1 and OPG. Bone Res ,2019, 7:18.
18. Liang G, Zhang Y. Genetic and epigenetic variations in iPSCs: potential causes and implications for application. Cell Stem Cell. 2013; 13: 149–159.

19. Roubelakis MG, Pappa KI, Bitsika V, Zagoura D, Vlahou A, Papadaki HA, Antsaklis A, Anagnou NP. Molecular and proteomic characterization of human mesenchymal stem cells derived from amniotic fluid: comparison to bone marrow mesenchymal stem cells. Stem Cells Dev. 2007; 16: 931–952.
20. Zhang Y, McNeill E, Tian H, Soker S, Andersson KE, Yoo JJ, Atala A. Urine derived cells are a potential source for urological tissue reconstruction. J Urol. 2008; 180: 2226–2233.
21. Zhang D, Wei G, Li P, Zhou X, Zhang Y. Urine-derived stem cells: a novel and versatile progenitor source for cell-based therapy and regenerative medicine. Genes Dis. 2014; 1: 8–17.
22. Bodin A, Bharadwaj S, Wu S, Gatenholm P, Atala A, Zhang Y. Tissueengineered conduit using urine-derived stem cells seeded bacterial cellulose polymer in urinary reconstruction and diversion. Biomaterials. 2010; 31: 8889–8901.
23. Zhou T, Benda C, Dunzinger S, Huang Y, Ho JC, Yang J, Wang Y, Zhang Y, Zhuang Q, Li Y, Bao X, Tse HF, Grillari J, Grillari-Voglauer R, Pei D, Esteban MA. Generation of human induced pluripotent stem cells from urine samples. Nat Protoc. 2012 ;7: 2080-9.
24. Guan J, Zhang J, Li H, Zhu Z, Guo S, Niu X, Wang Y, Zhang C. Human urine derived stem cells in combination with beta-TCP can be applied for bone regeneration. PloS One. 2015; 10: e0125253.
25. Green TR, Fisher J, Matthews JB, Stone MH, Ingham E. Effect of size and dose on bone resorption activity of macrophages by in vitro clinically relevant ultra high molecular weight polyethylene particles. J Biomed Mater Res. 2000; 53: 490-7.
26. Zaveri TD, Dolgova NV, Lewis JS, Hamaker K, Clare-Salzler MJ, Keselowsky BG. Macrophage integrins modulate response to ultra-high molecular weight polyethylene particles and direct particle-induced osteolysis. Biomaterials. 2017; 115: 128-140.
27. Chen W, Bichara DA, Suhardi J, Sheng P, Muratoglu OK. Effects of vitamin E-diffused highly cross-linked UHMWPE particles on inflammation, apoptosis and immune response against S. aureus. Biomaterials. 2017; 143: 46-56.
28. Wu C, Chen L, Huang YZ, Huang Y, Parolini O, Zhong Q, Tian X, Deng L. Comparison of the Proliferation and Differentiation Potential of Human Urine-, Placenta Decidua Basalis-, and Bone Marrow-Derived Stem Cells. Stem Cells Int. 2018; 2018:7131532.
29. Yim N, Ryu SW, Choi K, Lee KR, Lee S, Choi H, Kim J, Shaker MR, Sun W, Park JH, Kim D, Heo WD, Choi C. Exosome engineering for efficient intracellular delivery of soluble proteins using optically reversible protein-protein interaction module. Nat Commun. 2016; 7: 12277.
30. Costa Verdera H, Gitz-Francois JJ, Schiffelers RM, Vader P. Cellular uptake of extracellular vesicles is mediated by clathrin-independent endocytosis and macropinocytosis. J Control Release. 2017; 266: 100-108.
31. Thery C, Amigorena S, Raposo G, Clayton A. Isolation and characterization of exosomes from cell culture supernatants and biological fluids. Curr Protoc Cell Biol. 2006; 3: 1-29.
32. Ormsby RT, Cantley M, Kogawa M, Solomon LB, Haynes DR, Findlay DM, et al. Evidence that osteocyte perilacunar remodelling contributes to polyethylene wear particle induced osteolysis. Acta Biomater. 2016, 33:242-51.

33. Chen L, Li L, Xing F, Peng J, Peng K, Wang Y, Xiang Z. Human Urine-Derived Stem Cells: Potential for Cell-Based Therapy of Cartilage Defects. Stem Cells Int. 2018; 2018: 4686259.
34. Bharadwaj S, Liu G, Shi Y, Wu R, Yang B, He T, Fan Y, Lu X, Zhou X, Liu H, Atala A, Rohozinski J, Zhang Y. Multipotential differentiation of human urine-derived stem cells: potential for therapeutic applications in urology. Stem Cells. 2013; 31: 1840-56.
35. Colombo M, Raposo G, Théry C. Biogenesis, Secretion, and Intercellular Interactions of Exosomes and Other Extracellular Vesicles. Annu Rev Cell Dev Biol. 2014; 30: 255-89.
36. Zawawi MS, Marino V, Perilli E, Cantley MD, Xu J, Purdue PE, Dharmapatni AA, Haynes DR, Crotti TN:Parthenolide reduces empty lacunae and osteoclastic bone surface resorption induced by polyethylene particles in a murine calvarial model of peri-implant osteolysis. J Biomed Mater Res A. 2015; 103:3 572-3579.
37. Nabeshima A, Pajarinen J, Lin TH, Jiang X, Gibon E, Cordova LA, Loi F, Lu L, Jamsen E, Egashira K, Yang F,Yao Z, Goodman SB: Mutant CCL2 protein coating mitigates wear particle-induced bone loss in a murine continuous polyethylene infusion model. Biomaterials. 2017; 117: 1-9.
38. Ormsby RT, Cantley M, Kogawa M, Solomon LB, Haynes DR, Findlay DM, Atkins GJ: Evidence that osteocyte perilacunar remodelling contributes to polyethylene wear particle induced osteolysis. Acta Biomater. 2016; 33: 242-251.
39. Delanois RE, Mistry JB, Gwam CU, Mohamed NS, Choksi US, Mont MA. Current Epidemiology of Revision Total Knee Arthroplasty in the United States. J Arthroplasty. 2017; 32: 2663–2668.
40. Gwam CU, Mistry JB, Mohamed NS, Thomas M, Bigart KC, Mont MA, Delanois RE. Current Epidemiology of Revision Total Hip Arthroplasty in the United States: National Inpatient Sample 2009 to 2013. J Arthroplasty. 2017; 32: 2088–2092.
41. Hu Y, Xu R, Chen CY, Rao SS, Xia K, Huang J, Yin H, Wang ZX, Cao J, Liu ZZ, Tan YJ, Luo J, Xie H. Extracellular vesicles from human umbilical cord blood ameliorate bone loss in senile osteoporotic mice. Metabolism. 2019; 95: 93-101.
42. Chen CY, Rao SS , Tan YJ, Luo MJ, Hu XK, Yin H, Huang J, Hu Y, Luo ZW, Liu ZZ, Wang ZX, Cao J, Liu YW, Li HM, et al. Extracellular vesicles from human urine-derived stem cells prevent osteoporosis by transferring CTHRC1 and OPG. Bone Res. 2019; 7: 18.
43. Guan J, Zhang J, Guo S, Zhu H, Zhu Z, Li H, Wang Y, Zhang C, Chang J. Human urine-derived stem cells can be induced into osteogenic lineage by silicate bioceramics via activation of the Wnt/β-catenin signaling pathway. Biomaterials. 2015; 55: 1-11.
44. Xu S, Liu C, Ji HL. Concise Review: Therapeutic Potential of the Mesenchymal Stem Cell Derived Secretome and Extracellular Vesicles for Radiation-Induced Lung Injury: Progress and Hypotheses. Stem Cells Transl Med. 2019; 8: 344-354.
45. Zheng G, Huang R, Qiu G, Ge M, Wang J, Shu Q, Xu J. Mesenchymal stromal cell-derived extracellular vesicles: regenerative and immunomodulatory effects and potential applications in sepsis. Cell Tissue Res. 2018; 374: 1-15.

46. Lener T, Gimona M, Aigner L, Borger V, Buzas E, Camussi G, et al. Applying extracellular vesicles based therapeutics in clinical trials - an ISEV position paper. J Extracell Vesicles. 2015; 4: 30087.
47. Zhang Y, Chopp M, Meng Y, Katakowski M, Xin H, Mahmood A, Xiong Y. Effect of exosomes derived from multipluripotent mesenchymal stromal cells on functional recovery and neurovascular plasticity in rats after traumatic brain injury. Journal of neurosurgery. 2015; 122: 856-867.
48. Cuetara BL, Crotti TN, O'Donoghue AJ, McHugh KP. Cloning and characterization of osteoclast precursors from the RAW264.7 cell line. In Vitro Cell Dev Biol Anim. 2006; 42: 182-8.
49. Li CJ, Cheng P, Liang MK, Chen YS, Lu Q, Wang JY, Xia ZY, Zhou HD, Cao X, Xie H, Liao EY, Luo XH. MicroRNA-188 regulates agerelated switch between osteoblast and adipocyte differentiation. J Clin Invest.2015; 125: 1509-1522
50. Xie H, Cui Z, Wang L, Xia Z, Hu Y, Xian L, Li C, Xie L, Crane J, Wan M, Zhen GH, Bian Q, Yu B, Chang WZ, Qiu T, Pickarski M, Duong LT, Windle JJ, Luo XH, Liao EY, Cao X. PDGF-BB secreted by preosteoclasts induces angiogenesis during coupling with osteogenesis. Nat. Med. 2014; 20: 1270–1278.

Figures

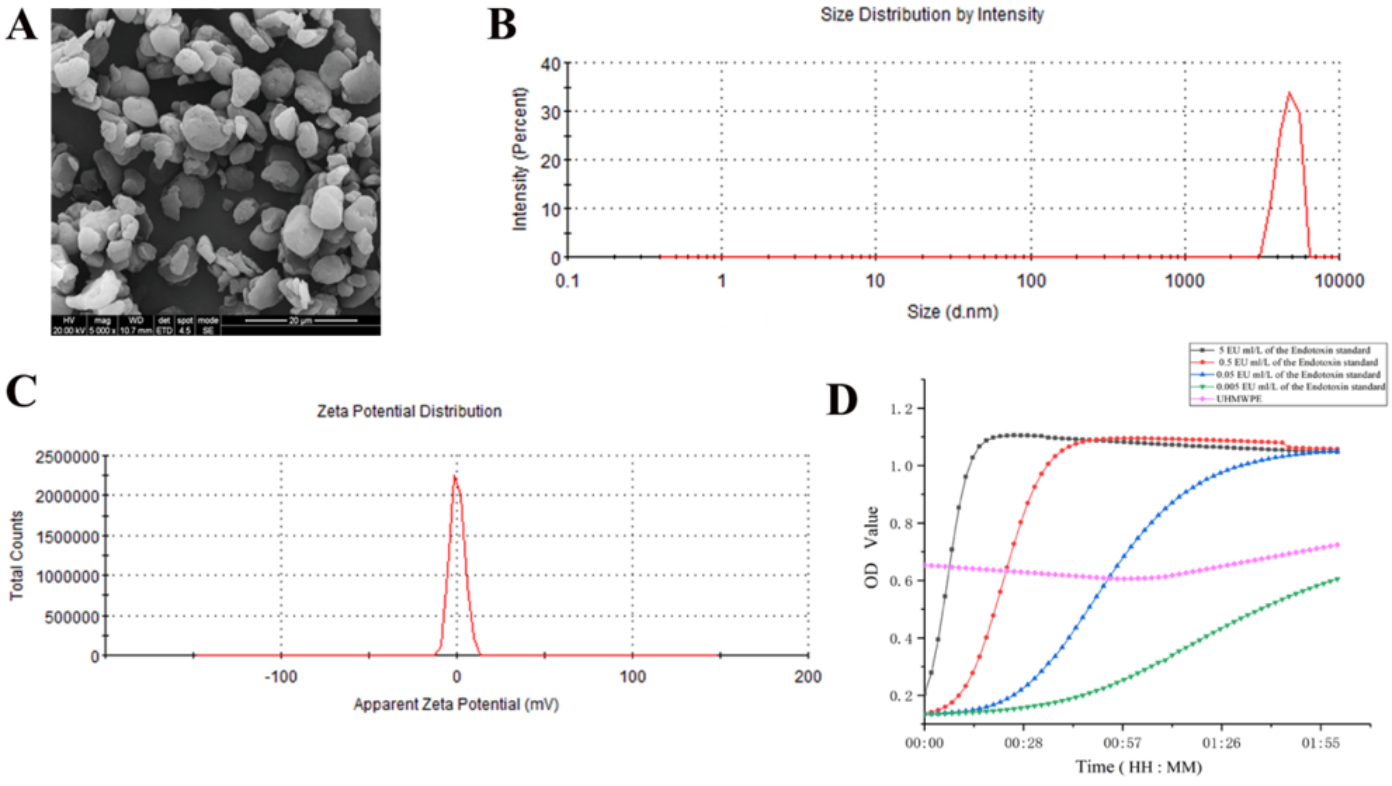

Figure 1

UHMWPE microparticle characterization. (A) SEM image of UHMWPE microparticles (scale bar 20 μm) showing the size distribution and shape of the UHMWPE microparticles. (B) (C) Microparticles were

analyzed for size distribution and Zeta distribution using DLS. (D) Analysis curve of endotoxin on UHMWPE.

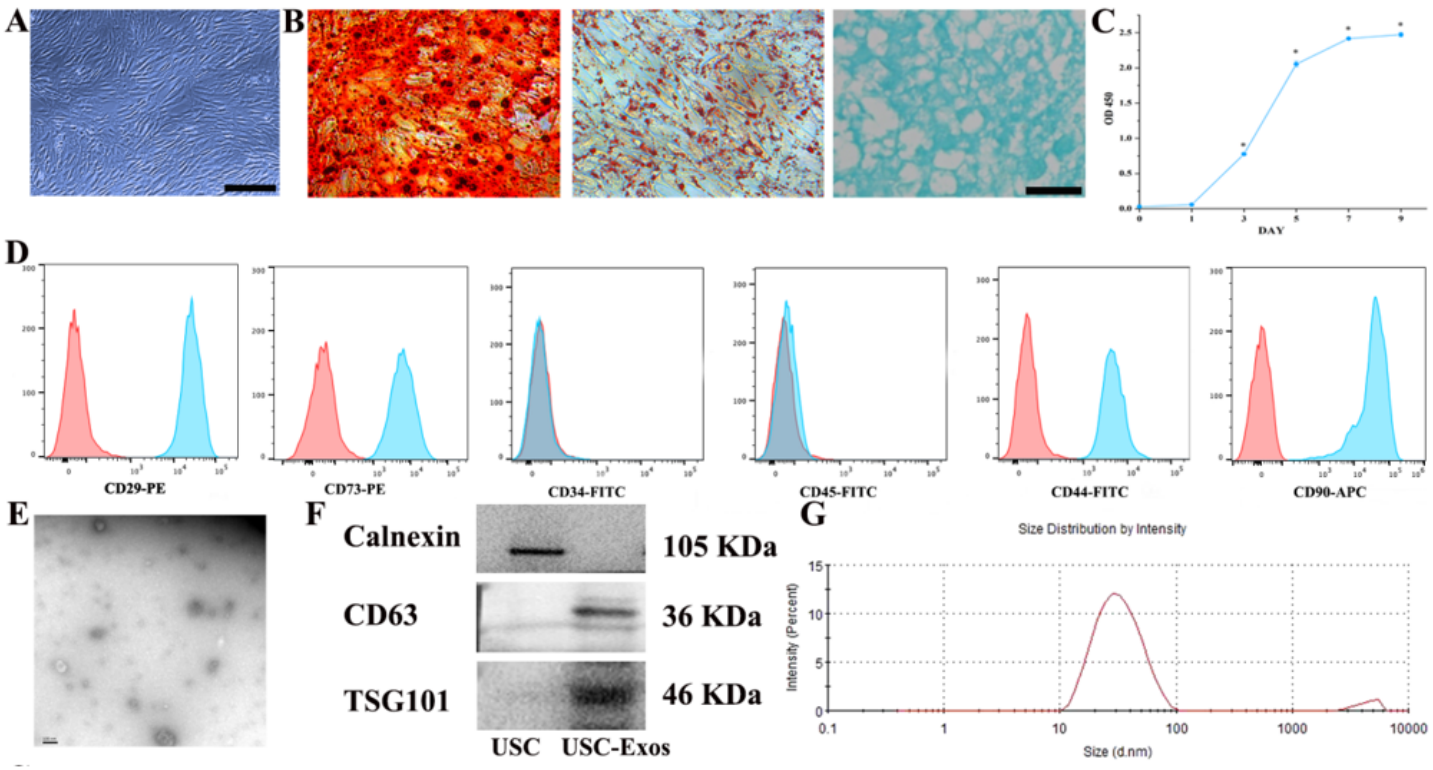

Figure 2

Identification of USCs and USC-Exos. (A) USCs showed a spindle-like morphology. Scale bar: 100 μm. When cultured in osteogenic, adipogenic or chondrogenic medium, USCs were able to differentiate into osteoblasts, adipocytes or chondrocytes, as evidenced by Alizarin Red S staining (B-a; Scale bar: 100 μm), Oil Red O staining (B-b; Scale bar: 100 μm) and Alcian Blue staining (B-c; Scale bar: 100 μm), respectively. (C) USCs growth curve. (D) Flow cytometry analysis of the typical surface markers in USC-Exos. (E) Morphology of USC-Exos under transmission electron microscopy, and western blot analysis of exosomal markers in USC-Exos and USCs. Scale bar: 100 nm. (F) Flow cytometry analysis of the cell surface markers on USCs. (G) USC-Exos size distribution measured by DLS analysis.

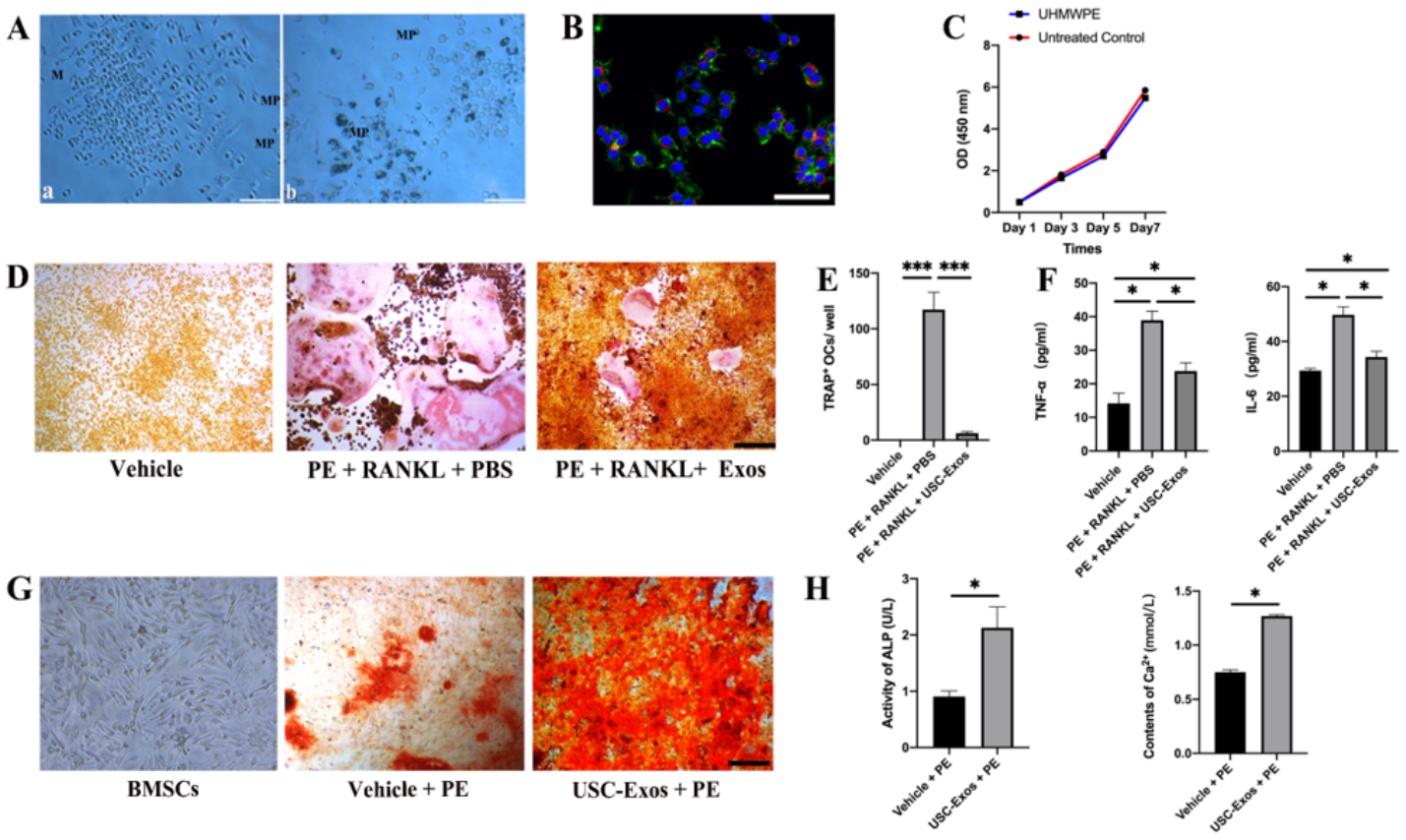

Figure 3

USC-Exos promote osteogenesis and inhibit osteoclast formation. (A) UHMWPE particles (dark dots) were internalized in the macrophage cells (MP). (B) Representative immunofluorescence images showing the internalization of PKH26-labeled USC-Exos (red) by RAW264.7 stained with phalloidine (green). Cell nuclei were stained with DAPI (blue). White arrows indicate exosomes (red). Scale bars = 50 μm. (C) Macrophages exposed to UHMWPE particles for 1 - 7 days. Macrophage proliferation was measured 1, 3, 5 and 7 days after particle exposure. (D) Osteoclast differentiation of RAW264.7 cells visualized by TRAP staining. Scale bar: 200 μm. (E) The numbers of TRAP+ multinucleated (> 3 nuclei) osteoclasts in each well of a 48-well plate were counted. n = 3 per group. ***P<0.001. (F) The concentration of TNF-α and IL-6 in conditioned media from RAW264.7 cells receiving different treatments was determined by ELISA. n=3 per group. *P<0.005. (G) Alizarin red S (ARS) staining of mineralized nodules of MSCs receiving different treatments under osteogenic inductive conditions. (H) Quantitative analyses of ALP and Ca2+ in conditioned media from BMSCs receiving different treatments. n = 3 per group. *P<0.05.

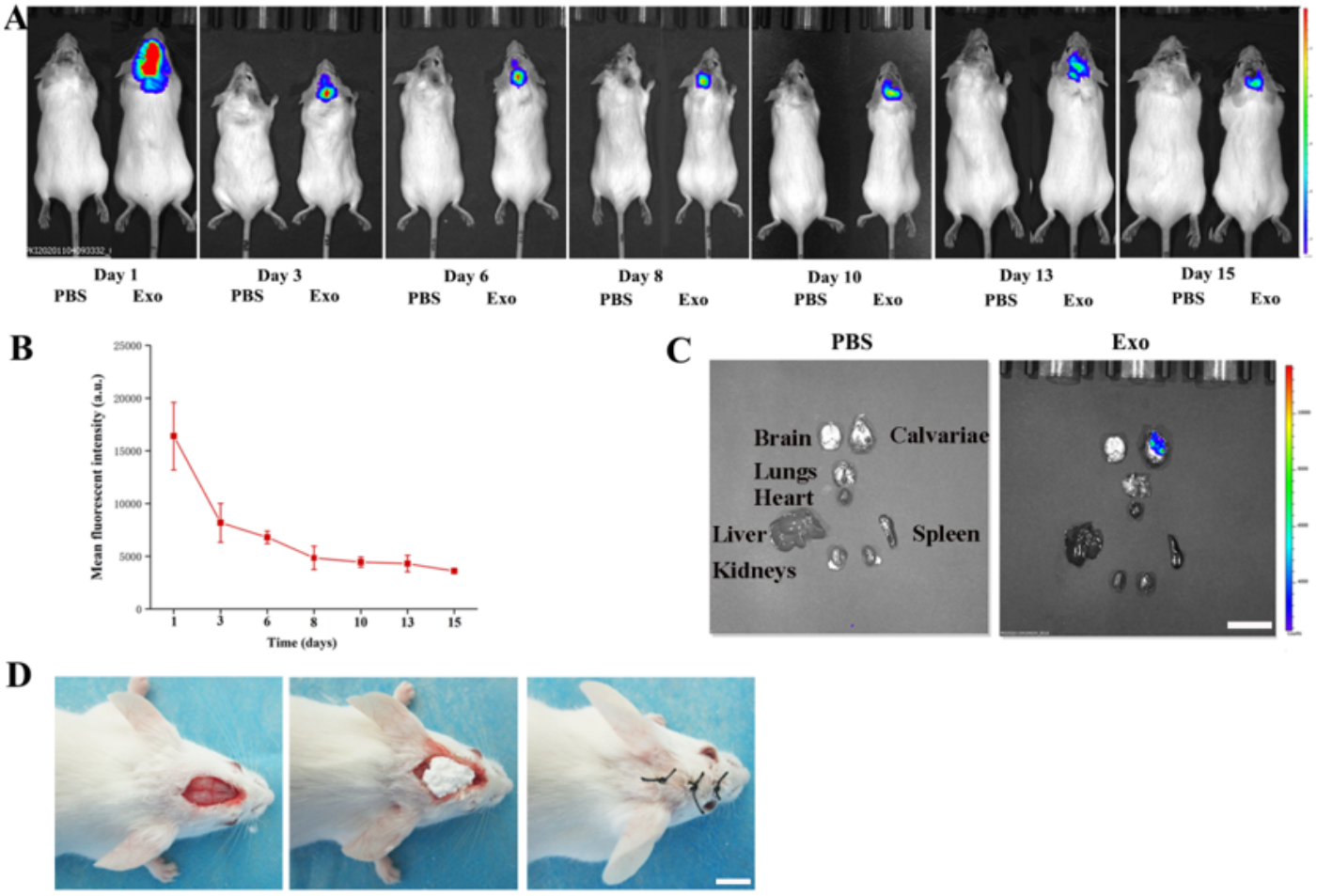

Figure 4

USC-Exos accumulation in mice.. (A) Gross view of air pouches dissected from mice 7 days after bone implantation. (B) The DiR-labelled USC-Exos were local injected into the mice air pouch and then these mice were imaged by IVIS at indicated time.(C) 14 days after injection, the mice were sacrificed and mouse organs (heart, lungs, liver, spleen and kidneys) were taken out for imaging. Scale bar: 50 μm. (D) The surgical protocol of mouse osteolysis model. Scale bar: 30 μm.

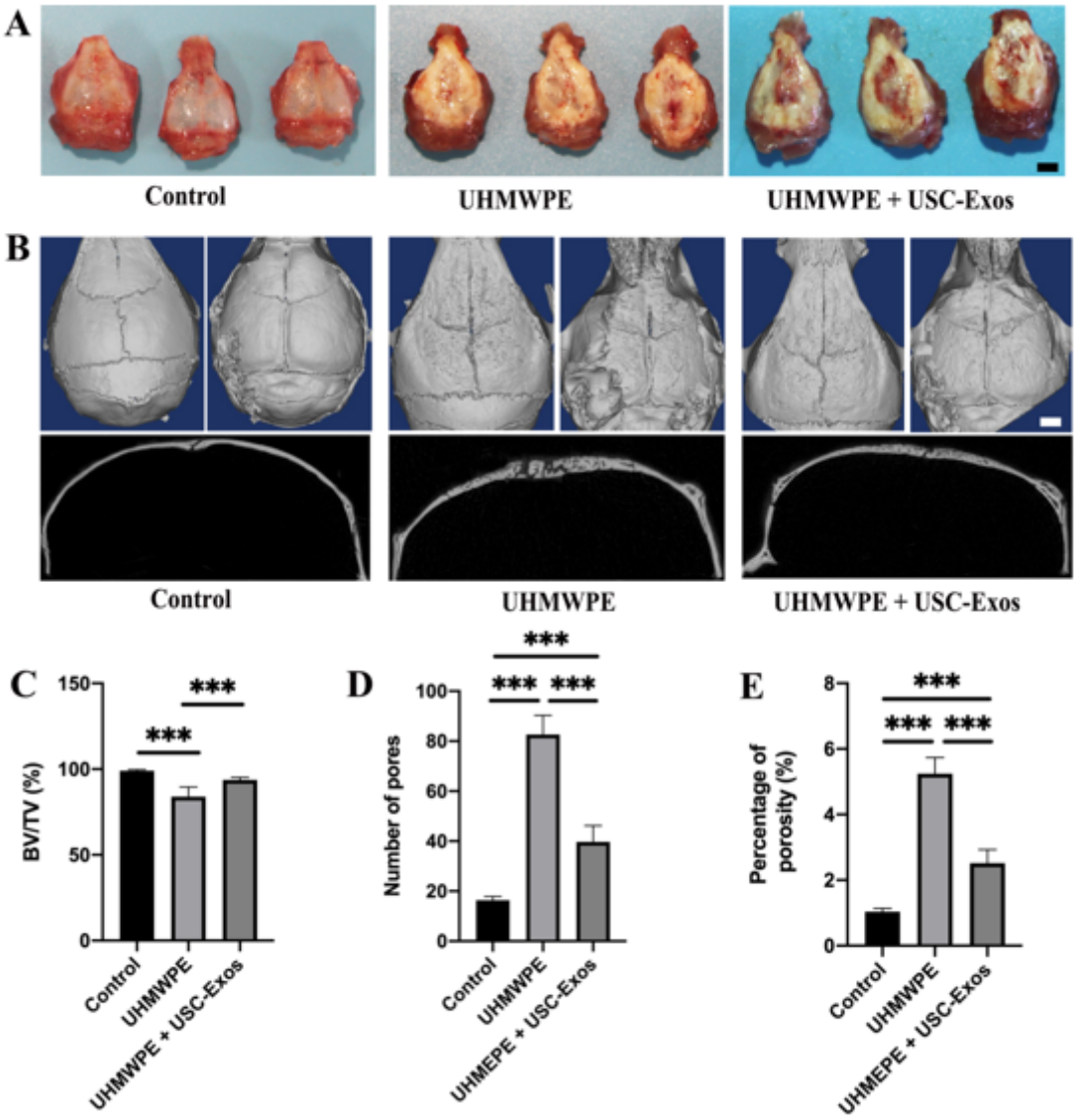

Figure 5

USC-Exos attenuates bone loss in osteolysis mice. (A) Typical macroscopic appearance of the calvariums dissected from mice 4 weeks postoperation. (B) Quantitative μCT analyses of bone architecture parameters including bone volume/total tissue volume (BV/TV) (C), number of pores (D) and percentage of porosity (E), n=4 or 5 per group. ***P < 0.05. Scale bar: 30 μm.

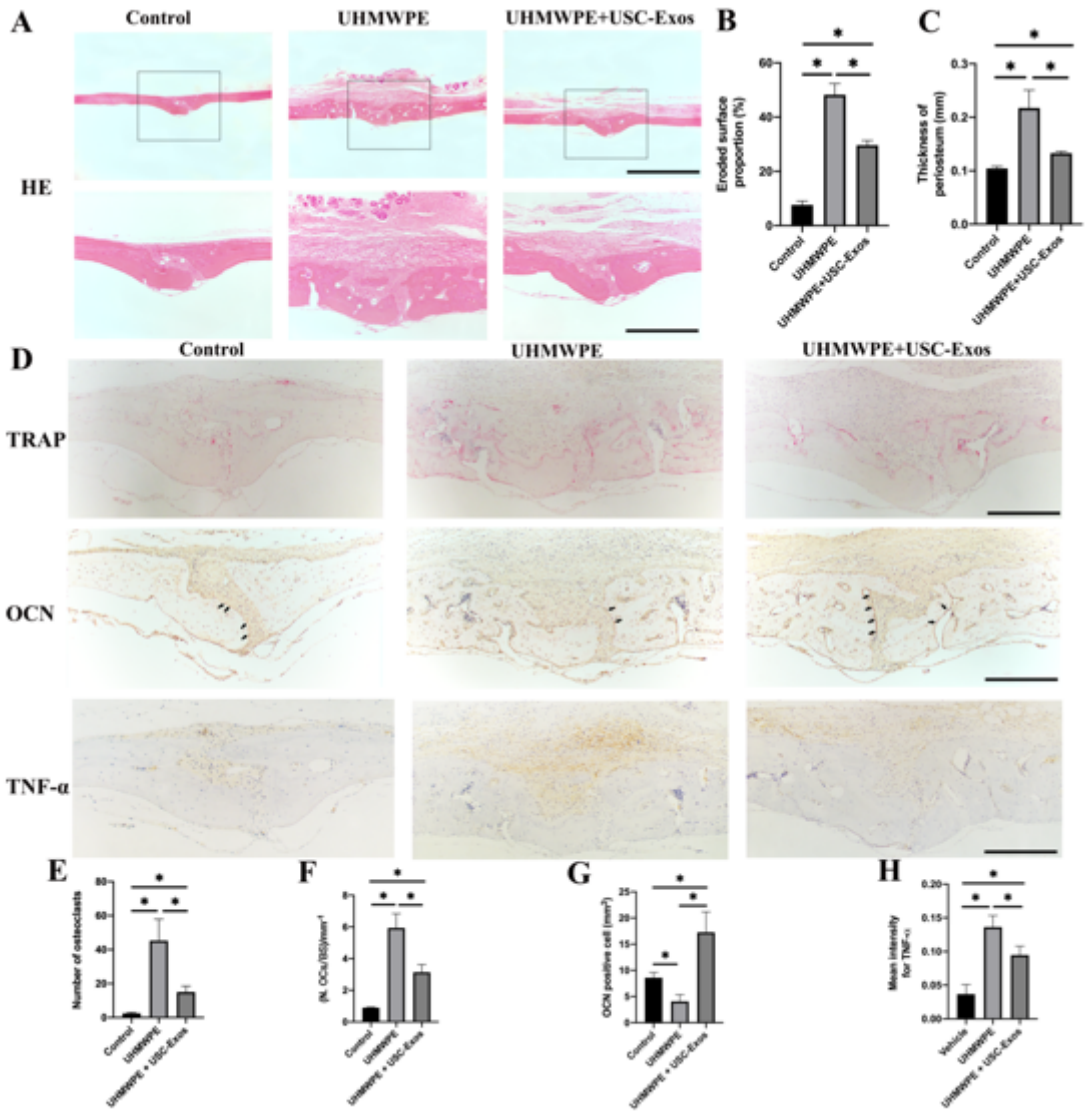

Figure 6

USC-Exos inhibits chronic inflammation and osteoclastic activities in vivo. (A) H&E staining staining of the calvaria tissue sections. Scar bar : 100 μm. Histomorphometric evaluation of the (B) eroded surface area, (C) periosteum thicknes within the ROI in each group were measured. n = 4 or 5 per group. *p < 0.05 compared to the Vehicle group. Statistical significance was determined by one-way ANOVA and two-sided Student's t-test. All data are shown as the mean ± SD. (D) Representative images of TRAP, OCN and TNF-α in vivo (brown, indicated by black arrows), quantitated using Image Pro Plus 6. Scale bar = 100 μm. Histomorphometric evaluation of the number of (E) TRAP-positive osteoclasts (purple, indicated by black arrows), and (F) percentage of osteoclast surface per bone surface (OCs/BS, %). Quantitative analysis of OCN (G) and TNF-α (H) expression for each sample (n = 4 or 5 per group). All data presented as means ± SEM. *P < 0.05.

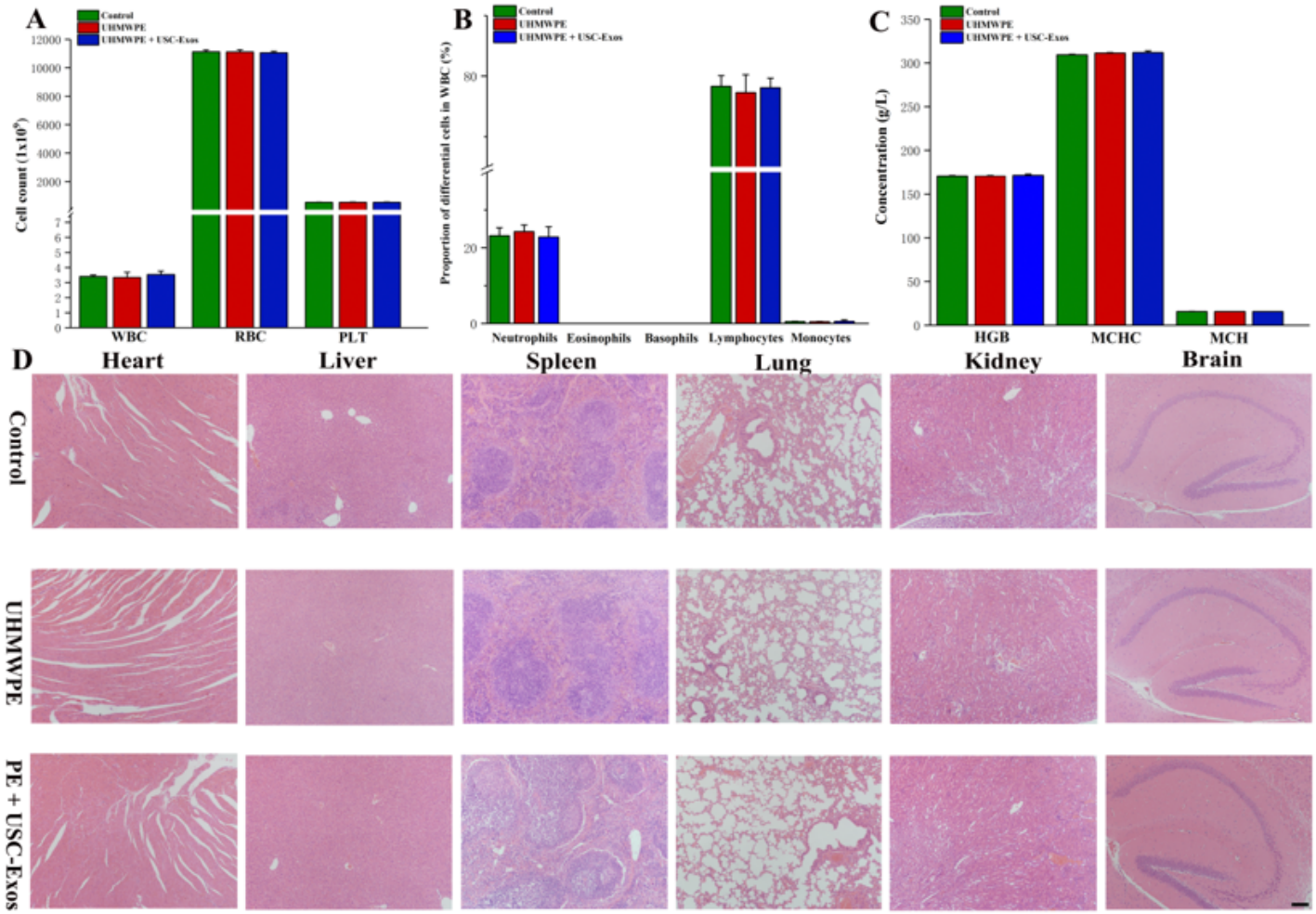

Figure 7

Biocompatibility and safety of USC-Exos. (A) Complete cell counts (white blood cells, red blood cells and platelets) in the untreated, control and USC-Exos groups; n=10. *P<0.05 compared with the control groups. (B) Proportions of differential white blood cells in the untreated, control and USC-Exos groups; n=10. *P<0.05 compared with the control and UHMWPE groups.(C) Blood routine examination parameters in the untreated, control and USC-Exos groups; n=10. *P<0.05 compared with the control and UHMWPE groups. (D) H&E staining of major organs in different groups; scale bar, 100 μm.

Supplementary Files

This is a list of supplementary files associated with this preprint. Click to download.

- Scheme1.png
- SupplementaryFigures.docx